INVESTIGATION OF RANDOM AND FIXED PATTERN NOISE IN HIGH DISPERSION IUE SPECTRA

Saul J. Adelman[1,2] and David S. Leckrone[2]

Laboratory for Astronomy and Solar Physics
NASA Goddard Space Flight Center
Greenbelt, MD 20771

---

[1] NRC-NASA Research Associate

[2] Guest Investigator with the International Ultraviolet Explorer Satellite which is sponsored and operated by the National Aeronautics and Space Administration, by the Space Research Council of the United Kingdom, and by the European Space Agency; Guest Investigator at the Regional Data Analysis Facility of NASA Goddard Space Flight Center

SUMMARY

To obtain ultraviolet data with suitably high signal-to-noise ratios for quantitative spectral analyses, we composited IUE spectra for six sharp-lined normal B and A stars. As IUE detectors have limited dynamic ranges, we obtained three images in both the SWP and LWR cameras at each of three different exposure levels. Coaddition of these images reduces random noise (RN). For three stars, an image at each exposure level was taken at each of three different positions in the large aperture, thus causing the stellar spectra to be displaced relative to the background of fixed pattern noise (FPN). Images of the other stars were taken with the small aperture over a period of a month. If FPN varies slowly in a time scale of a few weeks, then coaddition of these spectra also should reduce FPN. We examined two well-exposed orders of each camera for all six stars. By shifting the stellar features of each exposure into coincidence

with the coadded spectrum and subtracting, we obtained difference spectra with components of both RN and FPN. Analyses of these difference spectra for the images taken with the large aperture produced a best estimate of RN = 4% and FPN = 6% on a single well-exposed image. These values reflect a 3-data point (2.1 pixel) smoothing. The signal-to-noise ratios of the coadditions produced from large aperture images are about twice those of single well-exposed images.

I. INTRODUCTION

To obtain ultraviolet data with suitably high signal-to noise ratios for quantitative spectral analyses, we have added together numerous high dispersion IUE exposures for each of six normal sharp-lined Population I B and A type stars. These stars are not known to be either photometric or spectroscopic variables. In this paper, we discuss our techniques and assess the amount of both random noise (RN) and fixed pattern noise (FPN) in both individual and averaged images. In IUE exposures, FPN is a low amplitude instrumental signal superimposed on the image. It may be variable on a scale of months and at a given time has a definite spatial and amplitude distribution on the surface of the detector. We assume that Gaussian statistics are appropriate to describe its amplitude distribution. Random noise is the result of photon statistics. There is also a contribution to RN due to errors in the placement of the beam as it is moved to read out the next pixel (Holm 1982). The images are also affected by microphonics due a ringing in the camera while the

camera is read as well as data transmission problems and cosmic rays. We did not study spectral regions of images obviously affected by such problems. Our exposure times are sufficiently short that there are few if any cosmic ray signatures in our data.

Our choice of sharp-lined early type stars, which was made to simplify the task of synthesizing lines in the complex ultraviolet spectra, is not ideal for studying noise. For the latter, the spectra of rapidly rotating stars, in which the noise and spectral feature frequencies are better separated, would be a more desirable choice. However, data for such stars suitable for coadding in the manner described in this paper have not been obtained.

II. THE OBSERVING PROCEDURES

As the IUE detectors, which are SEC Vidicon cameras, have limited dynamic ranges, we obtained high dispersion images in both the SWP and LWR cameras at three different exposure times to achieve adequate exposure levels over the entire wavelength ranges of the IUE spectrographs. To be able to reduce noise we obtained three images at each of the three exposure times. For three stars, π Cet, 134 Tau, and ν Cap, we obtained images with the star centered in the small aperture to maximize the spectral resolution. To minimize FPN we took images at each exposure level of each camera at two week intervals. For our other three stars, 21 Aql, θ Leo, and o Peg, we used the large aperture and for each exposure time took images at three different spatial

positions. This shifted the pattern of FPN relative to the stellar spectrum. Table 1 contains the numbers of high dispersion images we obtained for each star and used in this analysis.

The images we studied were the extracted spectral (MEHI) files which were processed from the raw data using the IUESIPS Version 2 software (Turnrose and Thompson 1984), the standard IUE project software with standard ITFs for each camera. Our images are not affected by any of the systematic errors discussed by Turnrose, Thompson, and Gass (1985). Thus we coadded images identically processed with the same software. As all the images of a given star were obtained within an interval of a few weeks, the camera sensitivities remained constant.

III. THE COADDITION PROCEDURES

For each star and camera, one exposure was adopted as reference, often one with an exposure time of middle duration. Then we determined the effective radial velocities of the other images, relative to this reference, by cross-correlating the central regions of selected well-exposed orders. Radial velocity offsets were caused by deliberate positional offsets in large aperture exposures and orbital Doppler shifts in both apertures. Before these cross-correlations were performed, the spectra were smoothed by a 3-point running boxcar routine to insure that spectral features rather than noise gave maxima in the correlation function. The IUE extraction routine oversamples the data. Each data sample point corresponds to a width of 0.707

pixels on the detector. 3-point smoothing increases the signal-to-noise per pixel by 1.46. In this paper we give results only for the smoothed data. We also measured the ratios of the apparent stellar fluxes to obtain relative exposure times. For small aperture exposures in particular, the fraction of total light passing through the aperture varied somewhat from image to image.

When we coadded the fluxes from different images, we used the relative exposure times as weights. But fluxes derived from using the extrapolated intensity transfer function had their relative exposure times divided by 10 and values clearly affected by microphonics or reseaus had their relative exposure times divided by 1000. Saturated fluxes were given zero weight. Even when the local continuum values were overexposed and not used, values from the line cores might be properly exposed, especially in the long wavelength ends of both cameras where they are most sensitive. Hence our technique of coaddition tends to equalize the numbers of photons included in the coaddition at wavelengths corresponding to the continuum and line cores for the middle and longward portions of the spectral ranges for the IUE cameras.

IV. THE NOISE INVESTIGATION PROCEDURES

For the present investigation we examined two orders of each camera for all six stars (orders 89 and 80 for SWP and orders 98 and 91 for LWR). These orders were chosen so that, on the average, the first order had all of the exposures contributing to the coaddition's continuum values and none were seriously

overexposed. For this order the images with the longest exposure times were well-exposed. The second order studied in each camera fell at longer wavelengths. In this latter case images with the longest exposure times were overexposed in the continuum, but not in the line cores. Usually the middle duration exposures were well-exposed while the shorter duration exposures were somewhat underexposed.

The basis of our noise investigation procedure for large aperature images is illustrated with a very simple example in Figure 1. We consider three images with the same exposure time. Here a single square represents a stellar line and the arrow represents a single FPN spike. Our exposures are taken at three positions in the large aperture (right, center, and left). This shifts the stellar spectrum within the image format. The fixed pattern noise is thus shifted relative to the stellar spectrum by about ± 30 km s^{-1}. Column 1 of figure 1 shows the resulting displacements in FPN in the three exposures when the stellar features are brought into wavelength coincidence. At the bottom of column 1, we show the results of adding the three spectra so aligned. There are now three identical noise spikes with one-third the amplitude of the original spike. Two of them are displaced symmetically from the central position. Random noise is not depicted in the figure for the sake of simplicity. Let a and b be the amplitudes, as a fraction of the signal strength, of the coherent or fixed pattern noise and incoherent or random noise, respectively, in a single exposure. In our example, we have only one FPN spike while each image has a distribution of

such spikes. Then in the average of the spectra taken at these three positions in the large aperture, the mean amplitude of the fixed pattern noise at those positions where it occurs is

$$\sigma_{fp} = \sqrt{\{3(a/3)^2\}} = a/\sqrt{3} \qquad (1)$$

and the amplitude of the random noise is

$$\sigma_r = b/\sqrt{3}. \qquad (2)$$

We are assuming here that the fixed pattern noise has a random amplitude and a random spatial distribution yet is unchanged between images and can be studied by applying Gaussian statistics.

Column 2 of figure 1 shows the results of subtracting the average spectrum from each individual spectrum with the stellar features in coincidence. In these difference spectra, the stellar line has disappeared. Two of the three noise spikes in each difference spectra are negative echoes of the original spike with one-third of its amplitude while the third has a positive amplitude two-thirds of the original spike.

For this case

$$\sigma_{fp} = a\sqrt{\{2(1/3)^2+(2/3)^2\}} = 0.82a \qquad (3)$$

or a decrease in FPN. As we have a difference spectrum, the random noise has increased with

$$\sigma_r = b\sqrt{(1+3^{-1})}. \qquad (4)$$

When we combine these two sources of noise we find the total noise amplitude

$$\sigma_t = \sqrt{\{(0.82a)^2+(1.15b)^2\}} \qquad (5)$$

When we cross-correlate the left and right difference spectra with the central difference spectrum, the maximum

correlation occurs for the alignment seen in column 3 of Figure 1. Correlations come from the central noise spike as well as from some of the negative echoes. At the bottom of this column, we averaged these aligned difference spectra. The central spike has an amplitude two-thirds of that of the original spike and there are four negative echoes, two with an amplitude 0.11 and two with an amplitude 0.22 of the original spike.

For this average difference spectrum

$$\sigma_r = b\{\sqrt{(3+1)}\}/3 = 0.67\ b \tag{6}$$

and

$$\sigma_{fp} = \sqrt{\{(2a/3)^2 + 2(a/9)^2 + 2(2a/9)^2\}} = 0.75a \tag{7}$$

so

$$\sigma_t = \sqrt{\{(0.75a)^2 + (0.67b)^2\}} \tag{8}$$

If we now subtract the individual difference spectra in column 3 of figure 1 from the average difference spectrum, we obtain the results in column 4. The central noise spike has disappeared and we are left with four reduced amplitude noise spikes. For the left and right cases

$$\sigma_{fp} = \sqrt{\{\ 2(a/9)^2 + 2(2a/9)^2\}} = 0.35a \tag{9}$$

and for the central case

$$\sigma_{fp} = \sqrt{\{4(a/9)^2\}} = 0.22a. \tag{10}$$

Thus we use as an average $\sigma_{fp} = 0.31a$.

For all three cases

$$\sigma_r = \sqrt{\{b^2 + (b^2/3) + b^2([3+1]/3^2)\}} = 1.33\ b. \tag{11}$$

Hence,

$$\sigma_t = \sqrt{\{(0.31a)^2 + (1.33b)^2\}} \tag{12}$$

Typically for each camera we obtained a 3 x 3 array of

images corresponding to three spatial positions in the large aperture and three exposure levels at each position. If we assume that the ratio of FPN amplitude to exposure level is constant, regardless of exposure level, then the relative amplitude is preserved when we coadd the three images of different density obtained at a given position. Coaddition thus reduces the matrix to a set of three images, which correspond exactly to the case illustrated in figure 1 so that the values of σ_{fp} are as given above.

On the other hand RN is affected in a different manner when the nine images are averaged. As the relative exposure times were used as weights in the averaging process, RN is reduced in a manner appropriate to the number of equivalent images, n, with the same exposure time. For well-exposed orders of the final average image, n is usually about 6. This necessitates modifying equation (2) for the average spectrum to

$$\sigma_r = b\sqrt{n}, \tag{13}$$

equations (4) and (5) for the difference spectra to

$$\sigma_r = b\sqrt{(1+n^{-1})} \tag{14}$$

and (for n = 6)

$$\sigma_t = \sqrt{\{(0.82a)^2 + (1.08b)^2\}}, \tag{15}$$

equations (6) and (8) for the average difference spectra to

$$\sigma_r = b\ \{\sqrt{(n+1)}\}/n \tag{16}$$

and (for n = 6)

$$\sigma_t = \sqrt{\{(0.75a)^2 + (0.44b)^2\}}, \tag{17}$$

and equations (11) and (12) for the difference between the individual and average difference spectra to

$$\sigma_r = \sqrt{\{b^2+(b^2/n)+b^2([n+1]/n^2\}} \quad (18)$$

and (for n = 6)

$$\sigma_t = \sqrt{\{(0.31a)^2 + (1.17b)^2\}}. \quad (19)$$

We fit straight lines through both individual difference spectra (corresponding to column 2 of figure 1) and difference-average difference spectra (corresponding to column 4) to determine their respective noise amplitudes. Substituting these measured noise amplitude values in equations (15) and (19), respectively, allows a simultaneous solution for a and b. The values of a and b given in Table 2 are for the best determined cases. They suggest that for individual images the random noise amplitude in well-exposed regions is about 4% and the fixed pattern noise amplitude is about 6% of the average intensity. Thus in well-exposed orders the total noise amplitude in an individual spectrum is 7% of the signal or S/N = 14. Our estimate of RN is similar to that found by York and Jura (1982).

For our small aperture images, the stars could not shift in the aperture. If FPN were constant during the observations and neglecting the small Doppler shifts in the spectra due to spacecraft motion, then FPN would be subtracted out when the difference spectra are produced. Thus, to first order we can set a = 0 in equation (15) and thus

$$\sigma_t = 1.08b. \quad (20)$$

We fit straight lines through the difference spectra of π Cet, 134 Tau, and ν Cap and found σ_t. Table 3 shows the average σ_t values grouped by exposure time, restated in terms of b. These data yield $\langle b \rangle \simeq 0.05$ for the well-exposed orders. This

value is slightly larger than the average RN obtained for the large aperture images. Since there is no reason to believe that the actual RN should be different between large and small aperture exposures, we infer that variations in FPN over a period of one month have had the effect of increasing the noise amplitude in the small aperture difference spectra. When we cross-correlated the small aperture difference spectra, we found no sensible pattern. Any contribution due to changes in FPN over the period of a month has either been randomized sufficiently or has too small an amplitude so that we could not detect it.

V. NOISE IN THE AVERAGE SPECTRA

A major goal of this investigation was to evaluate the reduction in noise achieved by our coaddition procedures. In the average images, random noise is reduced by $1/\sqrt{n}$ where n is the number of well-exposed images. For π Cet, 134 Tau, and ν Cap, our small aperture cases, it is difficult to determine the values for a and b. An upper limit for b is 0.05 (see Table 3). We believe it appropriate to assume the same values as for the large aperture a = 0.06 and b =0.04. If so, then the random noise amplitude for both the large and the small aperture coadded spectra is 0.016.

So far we have neglected the relative Doppler shifts of stellar features and FPN due to spacecraft motion. This smears out the FPN and reduces its average amplitude in coadded spectra. Table 4 shows the average spacecraft motion for each star and camera and the rms deviation about this value.

Comparison of the mean of the σ's with the 7.2 km s^{-1} and 7.7 km s^{-1} widths of each pixel for LWP and for SWP, respectively, and allowance for our 3-point smoothing indicates this motion reduces the amplitude of FPN in coadded spectra obtained over a range of spacecraft velocities to about 83% of what its value would have been if the spacecraft had been stationary.

For the large aperture average spectra, the fixed pattern noise is also reduced by a factor of $\sqrt{3}$ as there are three stellar positions in the aperture. Its amplitude is thus $0.83 \times 0.060 / \sqrt{3} = 0.029$, which implies a total noise amplitude of 0.033 or S/N = 30.

For the small aperture case, we take the amplitude of FPN in coadded spectra to be the same as in individual images except for the 83% reduction due to Doppler smearing by spacecraft motion. Thus, FPN $\leq 0.83 \times 0.06 = 0.05$ and the total noise amplitude is ≤ 0.053 or S/N $\geq$ 19.

These results for large aperture coadded images indicate a factor of 2 improvement in signal-to-noise over the comparable 3-point smoothed well-exposed orders of individual images which have S/N = 14. These noise estimates are given for <u>average</u> fluxes and not with respect to the continuum. If they were given in such a manner, then the signal-to-noise values would increase by about a third.

Figures 2 and 3 show examples of these results for the SWP camera. The λλ1520-1540 region is shown for two stars with similar effective temperatures, π Cet, a small aperture case, and 21 Aql, a large aperture case. For both stars, an individual

well-exposed image is shown as well as the average of 9 images. The signal-to-noise ratio is clearly greater for the coadditions. FPN has been removed to a far greater extent in the large aperture case with the high frequency components being removed to a considerable extent.

The noise in the average spectra is dominated by fixed pattern noise. A possible approach to further reduce it is to take exposures at four different places in the large aperture rather than three. There is sufficient space to do so and not have the patterns of fixed pattern noise lie on top of one another. In this way one could reduce the FPN by an additional 15 %. A second approach is to obtain additional exposures after FPN has completely changed its characteristics. It is not clear what is the minimum time period for this to occur. Our results suggest a significant coherence in FPN in exposures taken a month apart. It is possibly safe to separate such sets of exposures by a year. For example, if another set of 3 images were obtained at each of our 3 exposure levels after a year had elapsed, these would possibly reduce FPN by up to 40%. This coupled with a further reduction in RN might reduce the total noise amplitude to 0.023, corresponding to S/N = 43.

An alternative possibility is that FPN is due to a slight misregistration of the ITF with time and hence is a function of camera temperature. For the images which we coadded, a variation of 2 to 3 K in camera temperature was seen.

Our analysis also ignores possible linearity errors. Oliversen (1984a,b) and Harris (1984) have discussed such

problems at low dispersion and their relation to the ITF. When one coadds spectra with different exposure levels, it is not clear whether such effects cancel or increase.

Our results differ from those of West and Shuttleworth (1981) who concluded that the summing of more than five high dispersion spectra is probably unwarranted. They used only images with the star centered in the aperture so that their summed image was most likely dominated by FPN. We avoided this difficulty by moving the star in the large aperture and so reduced FPN.

ACKNOWLEDGMENTS

We thank the IUE and Goddard RDAF staffs, in particular Mr. Keith Feggans, for their help in this investigation and Drs. Cathy Imhoff and Carol Grady for their comments on this paper. The cross-correlation routine was originally written by Dr. Sidney B. Parsons and the coaddition routine by Dr. F. H. Schiffer, III.

REFERENCES

Harris, A. W.: 1984, NASA IUE Newsletter 24, 42

Holm, A.: 1982, NASA IUE Newsletter 18, 10

Oliversen, N. A.: 1984a, NASA IUE Newsletter 24, 27

Oliversen, N. A.: 1984b, NASA IUE Newsletter 24, 50

Turnrose, B. E., Thompson, R. W.: 1984, "International Ultraviolet Explorer Imaging Processing Manual Version

2.0 (New Software)", CSC/TM-84/6058

Turnrose, B. E., Thompson, R. W., Gass, J. E.: 1985, NASA IUE Newsletter 25, 40

West, K., Shuttleworth, T.: 1981, ESA IUE Newsletter 12, 27

York, D. G., Jura, M.: 1982, Astrophys. J. 254, 88

Table 1: Number of Images Coadded

Star	Camera SWP	LWR
π Cet	9	7
134 Tau	10	8
ν Cap	8	7
21 Aql	9	9
o Peg	9	9
θ Leo	10	9

Table 3
Derived Average Noise Amplitudes from Small Aperture Images

Star	Well-Exposed Region	SWP 1542-1556	SWP 1716-1735	LWR 2326-2344	LWR 2530-2548
π Cet	Long	0.081↑	0.057	0.099↑	0.065
	Middle	0.056	0.041	0.067	0.044
	Short	0.066*	0.156*	0.056	0.080*
134 Tau	Long	0.093↑	0.083↑	0.103↑	0.071↑
	Middle	0.064	0.051	0.078↑	0.060
	Short	0.061	0.045*	0.054	0.059
ν Cap	Long	0.091↑	0.069↑	0.099↑	0.065
	Middle	0.047	0.036	0.067	0.044
	Short	0.045	0.042	0.056	0.089*

Notes: With different exposure times, the wavelengths which are properly exposed change. * = Overexposed and ↑ = underexposed, otherwise the regions measured are properly exposed.

Table 4
Spacecraft Motion Velocities

Star	Camera	Mean Velocity	Dispersion ($km\ s^{-1}$)	Range
π Cet	SWP	-28.2	±1.8	-25.6 to -30.0
	LWR	-27.4	±1.7	-25.7 to -29.6
ν Cap	SWP	+24.8	±1.2	+23.2 to +26.4
	LWR	+24.9	±1.1	+23.3 to +26.1
134 Tau	SWP	-26.3	±4.0	-20.9 to -31.5
	LWR	-26.3	±3.9	-21.7 to -31.4
o Peg	SWP	+20.1	±1.7	+17.1 to +21.7
	LWR	+19.9	±1.5	+17.1 to +20.9
21 Aql	SWP	+14.9	±4.2	+11.2 to +20.6
	LWR	+14.7	±4.2	+11.3 to +20.6
θ Leo	SWP	-26.1	±1.7	-23.7 to -28.2
	LWR	-25.8	±1.5	-23.8 to -27.9

Table 2
Fixed Pattern Noise and Random Noise Amplitudes
From Selected Large Aperture Images

Star	Camera	Well-Exposed Region	Number of Images	Wavelengths	Noise Amplitudes Fixed Pattern	Random
o Peg	SWP	Short	3	1526-1539	0.063	0.055
		Middle	3	1716-1735	0.062	0.036
		Short	2	1716-1735	0.061	0.043
	LWR	Middle	3	2326-2344	0.075	0.045
		Short	3	2326-2344	0.062	0.044
		Middle	3	2530-2548	0.080	0.038
θ Leo	SWP	Short	2	1542-1556	0.079	0.035
		Middle	3	1716-1735	0.052	0.042
	LWR	Short	3	2326-2344	0.052	0.043
		Middle	2	2326-2344	0.078	0.046
21 Aql	SWP	Short	3	1542-1556	0.073	0.030
		Middle	3	1716-1735	0.043	0.040
		Long	3	1716-1735	0.071	0.047
	LWR	Short	2	2326-2344	0.032	0.042
		Middle	2	2326-2344	0.066	0.049
Average	SWP				0.063	0.041
	LWR				0.064	0.044

Notes: The column 'Well-Exposed Region' indicates approximately where this region occurs for the spectra under consideration. 'Wavelengths' indicates where the measurements were made.

Figure Captions

Figure 1: We illustrate our procedure to reduce fixed pattern noise schematically with a single square stellar line and a single fixed pattern noise (FPN) spike, the arrow. Our exposures are taken at three places in the large aperture (left, center, and right). Column 1 shows the resulting displacements in FPN in the three exposures when the stellar features are brought into coincidence. At the bottom of column 1 we show the result of coadding the three spectra so aligned. There are now three noise spikes with one-third of the amplitude of the original spike.

Column 2 shows the results of subtracting the average spectrum from each individual spectrum with the stellar features in coincidence. In these difference spectra, the stellar line has disappeared. Two of the three noise spikes in each difference spectra are negative echoes of the original spike with one-third of its amplitude while the third has a positive amplitude two-thirds of the original spike.

If we now cross-correlate the left and right difference spectra with the central difference spectra, we expect the alignment seen in column 3. Correlations come from the central spike as well as from some of the negative echoes. At the bottom of this column, we averaged these aligned difference spectra. The central spike has an amplitude two-thirds that of the original spike and there are four negative echoes with amplitudes of 0.11 and 0.22 of the original spike.

If we now subtract the individual difference spectra in column 3 from the average difference spectrum, we obtain the results in column 4. The central noise spike has disappeared and we are left with two negative and two positive spikes of 0.11 and 0.22 of the amplitude of the original spike.

The spectra in column 4 have significantly supressed FPN so that their noise amplitudes are largely dominated by RN. Thus by comparing the noise amplitudes of spectra in columns 2 and 4, we can estimate the separate amplitudes of FPN and RN. In our simple illustration, we have neglected the relative Doppler shifts of stellar features and FPN due to spacecraft motion. This smears out the FPN and reduces its average amplitude in coadded spectra.

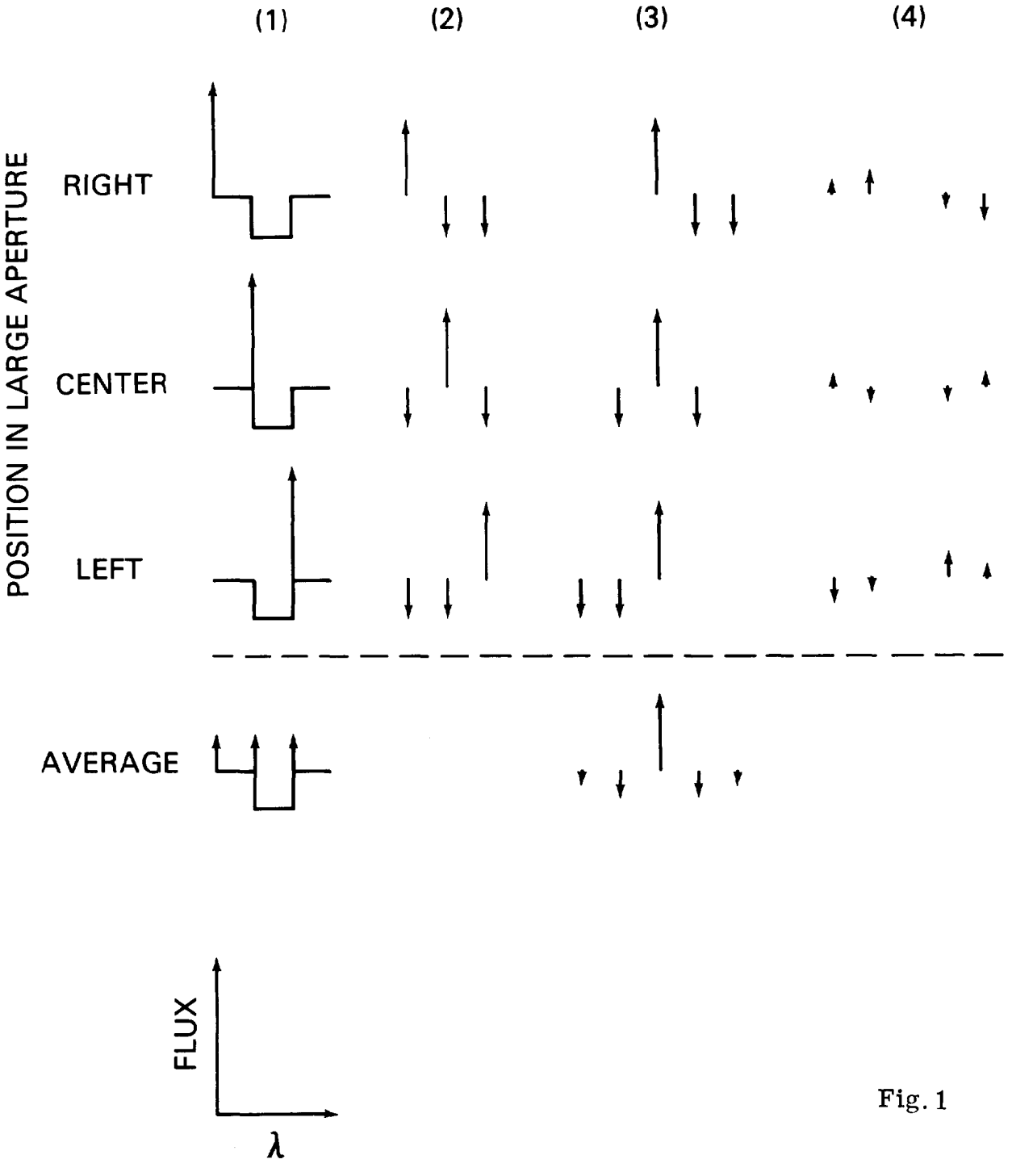
(1)
(2)
(3)
(4)
POSITION IN LARGE APERTURE
RIGHT
CENTER
LEFT
AVERAGE
FLUX
λ

Fig. 1

Figure 2: The λλ1520-1540 region in SWP 16248, a single small aperture high dispersion exposure of π Cet, and in the coadded spectrum. RN has been reduced in the coaddition relative to the individual images. However, as the individual images were taken in the same place in the aperture, the FPN of each image is similar.

Figure 3: The λλ1520-1540 region in SWP 19971, a single large aperture high dispersion exposure of 21 Aql, and in the coadded spectrum. Both RN and FPN have been reduced in the coaddition relative to the individual images. Comparison of figures 2 and 3 shows that taking exposures with the star in several places in the large aperture is a method of reducing FPN.

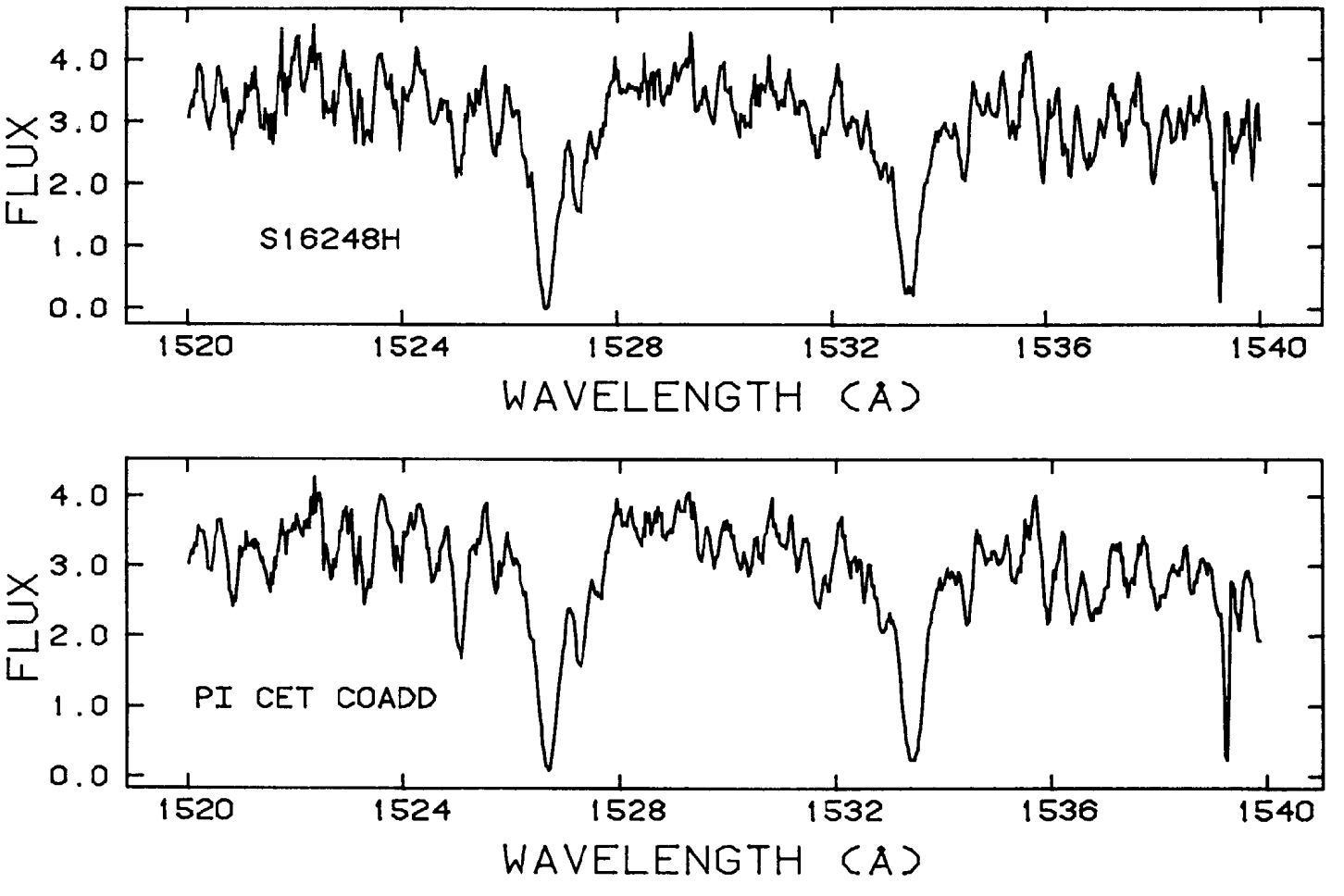
FLUX
4.0
3.0
2.0
1.0
0.0
S16248H
1520
1524
1528
1532
1536
1540
WAVELENGTH (Å)
FLUX
4.0
3.0
2.0
1.0
0.0
PI CET COADD
1520
1524
1528
1532
1536
1540
WAVELENGTH (Å)

Fig. 2

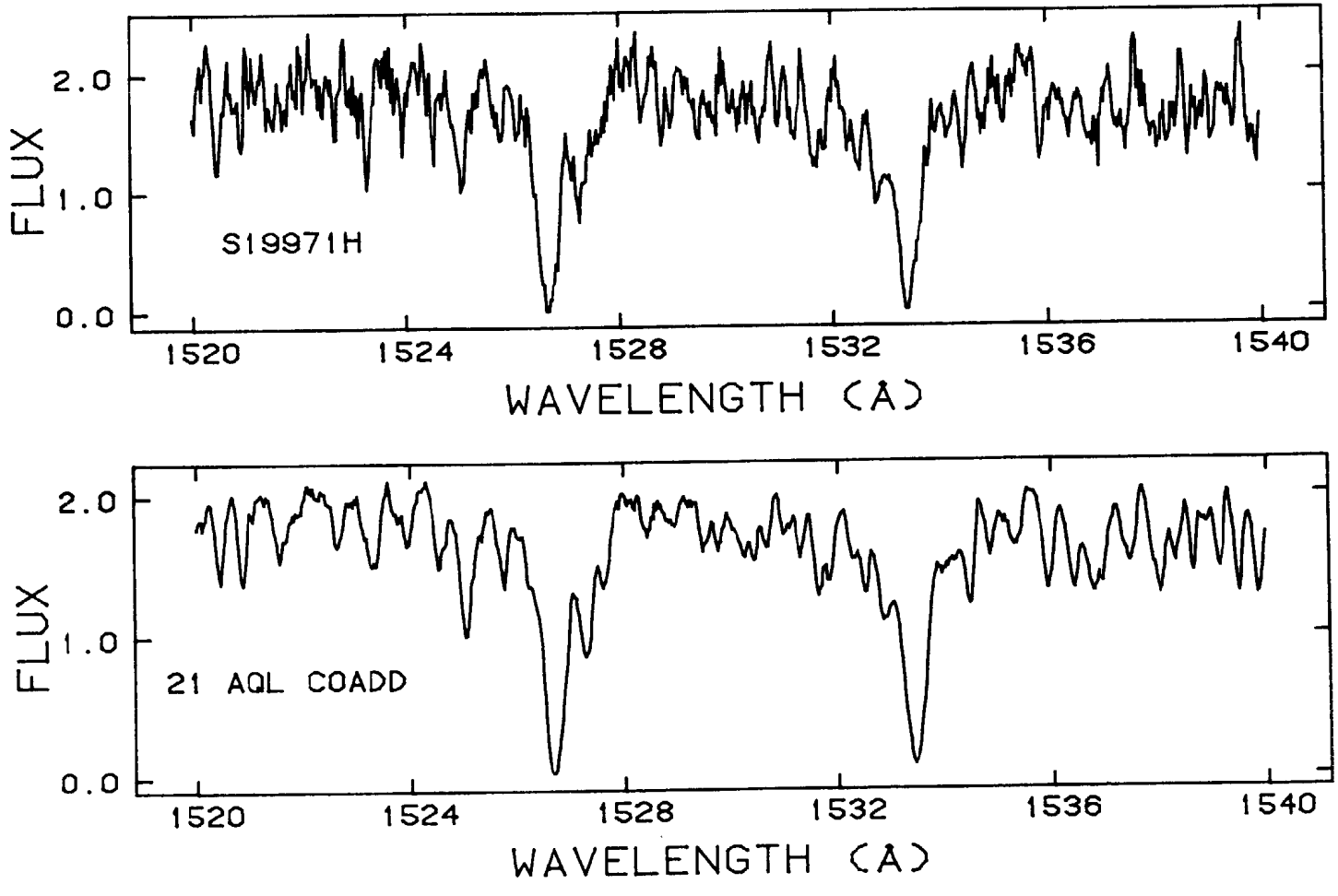
FLUX
2.0
1.0
0.0
S19971H
1520
1524
1528
1532
1536
1540
WAVELENGTH (Å)
FLUX
2.0
1.0
0.0
21 AQL COADD
1520
1524
1528
1532
1536
1540
WAVELENGTH (Å)

Fig. 3